Check for updates

Two boron atoms *versus* one: high-performance deep-blue multi-resonance thermally activated delayed fluorescence emitters†‡

Chin-Yiu Chan,§*[a] Subeesh Madayanad Suresh,§[b] Yi-Ting Lee,§[a]
Youichi Tsuchiya, [ID][a] Tomas Matulaitis,[b] David Hall,[bc] Alexandra M. Z. Slawin, [ID][b]
Stuart Warriner,[d] David Beljonne, [ID][c] Yoann Olivier, [ID][e] Chihaya Adachi [ID]*[af] and
Eli Zysman-Colman [ID]*[b]

Two new deep-blue narrowband multi-resonant emitters, 1B-DTACrs and 2B-DTACrs, one of which shows thermally activated delayed fluorescence (TADF), based on boron, nitrogen, and oxygen doped nanographenes are reported. Devices based on 2B-DTACrs showed an EQE_{max} of 14.8% and CIE coordinates of (0.150, 0.044), which are very close to the BT.2020 requirement for blue pixels.

Thermally activated delayed fluorescence (TADF) materials can achieve 100% internal quantum efficiency (IQE) by harvesting both singlet and triplet excitons. In 2012, Adachi and co-workers first reported organic light-emitting diodes (OLEDs) that showed IQEs of 100% based on organic donor–acceptor (D–A) type TADF emitters.[1] Successively, a wide variety of D–A type TADF emitters have been developed, resulting in devices showing high external quantum efficiencies (EQEs) of over 20% for blue, green, and red emission colors.[2–6] Nonetheless, D–A type TADF emitters usually possess broad emission bands that result in devices with poor color purity pixels. To achieve the BT.2020 standard for high-definition displays, narrowband electroluminescence (EL) in devices that show high EQE is highly desired.

Beyond the D–A type emitters, in 2016, Hatakeyama and co-workers first reported pure-blue boron-containing multi-resonance TADF (MR-TADF) emitters that feature narrowband emissions and high photoluminescence quantum yields (Φ_{PL}, PLQYs).[7] The narrowband emission behaviour of MR-TADF emitters is the most suitable for high-definition display with a wide colour gamut, *i.e.*, BT.2020 standard. Since then, the development of MR-TADF emitters has attracted much attention.[8–10] To date, there have been numerous reports on high-efficiency OLEDs based on MR-TADF emitters with blue, green, and red emissions.[8–13] Nonetheless, there are a limited number of reports on high-efficiency MR-TADF emitters that can fulfil the requirement of the colour gamut for the blue pixel, *i.e.*, Commission Internationale de lÉclairage coordinates (CIE$_{x,y}$) = (0.131, 0.046).[14] As a result, it is necessary to develop high-efficiency deep-blue MR-TADF emitters that satisfy the colour gamut requirement of the BT.2020 standard, *i.e.*, CIE$_y$ ≤ 0.05.

Here, we report two boron-based deep-blue emitters containing a mixed O/N donor atom system, one of which is MR-TADF. **1B-DTACrs** and **2B-DTACrs** were synthesized in five steps starting from 3,5-difluorobromobenzene. The key borylation reaction proceeded in 62% and 58% yield, respectively, for **1B-DTACrs** and **2B-DTACrs** from the common intermediate **4**. Site selective borylation was achieved by controlling the reaction temperature and the amount of BBr$_3$ in the reaction (Fig. 1). The identity and purity of both emitters were confirmed by a combination of ^{1}H NMR (Fig. S13 and S17, ESI†), ^{13}C NMR (Fig. S14 and S18, ESI†) spectroscopy, melting point determination, high-resolution mass spectrometry (Fig. S15 and S19, ESI†), single crystal X-ray diffraction (Fig. 1), and elemental analysis (Fig. S16 and S20, ESI†). **1B-DTACrs** and **2B-DTACrs** both display deep-blue narrowband emission at 440 and 447 nm and FWHMs of 30 and 26 nm, respectively, in the device. However, **1B-DTACrs** is TADF-inactive while **2B-DTACrs** is TADF-active. Devices based on **1B-DTACrs** and **2B-DTACrs**

[a] *Center for Organic Photonics and Electronics Research (OPERA), Kyushu University, Motooka, Nishi, Fukuoka 819-0395, Japan.*
  E-mail: chinyiu.chan@opera.kyushu-u.ac.jp

[b] *Organic Semiconductor Centre, EaStCHEM School of Chemistry, University of St Andrews, St Andrews, KY16 9ST, UK. E-mail: eli.zysman-colman@st-andrews.ac.uk*

[c] *Laboratory for Chemistry of Novel Materials, University of Mons, 7000, Mons, Belgium*

[d] *School of Chemistry, University of Leeds, Woodhouse Lane, Leeds, UK*

[e] *Laboratory for Computational Modeling of Functional Materials, Namur Institute of Structured Matter, Université de Namur, Rue de Bruxelles, 61, B-5000 Namur, Belgium*

[f] *International Institute for Carbon Neutral Energy Research (I2CNER), Kyushu University, 744 Motooka, Nishi, Fukuoka 819-0395, Japan.*
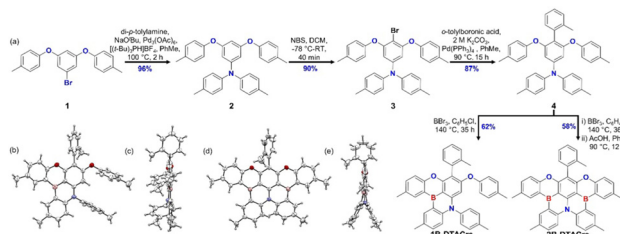 *E-mail: adachi@cstf.kyushu-u.ac.jp*

Fig. 1 (a) Synthetic route of **1B-DTACrs** and **2B-DTACrs**. ORTEP view of **1B-DTACrs** and **2B-DTACrs**; (b) plane view and (c) side view of **1B-DTACrs**, (d) plane view and (e) side view of **2B-DTACrs**. Thermal ellipsoids are displayed at 50% probability.

demonstrated maximum external quantum efficiencies (EQE_{max}) of 1.3 and 14.8%, respectively, together with corresponding CIE coordinates of (0.154, 0.049) and (0.150, 0.044), which are very close to the BT.2020 standard, *i.e.*, (0.131, 0.046).

Crystals for **1B-DTACrs** were obtained by slow diffusion of hexane into a saturated solution of the emitter in THF. Crystals of **2B-DTACrs** were obtained directly from a temperature gradient sublimation method (Fig. 1). The ditolylamine (DTA) unit adopts a propeller structure. In the case of **1B-DTACrs**, where there is only one boron in the compound, the MR-TADF core remains nearly planar. The *o*-tolyl unit is approximately perpendicular to the aromatic core in both emitters. Yasuda and co-workers reported **BSBS-N1**,[15] a structurally analogous sulfur-containing compound to **2B-DTACrs**, which was described as having a highly distorted structure, whereas **2B-DTACrs** possesses a nearly planar geometry at the B,O-substituted pentacene core with an out-of-plane alignment of two aryl rings of the DTA unit.[15] There are no significant intermolecular π–π interactions in the solid state for either compound, which may be a consequence of the orthogonally disposed *o*-tolyl unit.

The ground- and excited-state properties of **1B-DTACrs** and **2B-DTACrs** were modelled using DFT and spin-component scaling second order approximate coupled-cluster (SCS-CC2) methods, respectively (Fig. 2). Both compounds possess difference density distributions between the ground and excited-state reminiscent of other MR-TADF emitters.[10] Addition of the second boron atom in **2B-DTACrs** resulted in a small stabilization in the HOMO and LUMO energy levels compared to those of **1B-DTACrs** and a corresponding small decrease (0.12 eV) in the band gap (Fig. 2(a)). The S_1 state is stabilized from 3.38 eV in **1B-DTACrs** to 3.27 eV in **2B-DTACrs**, while the T_1 states are essentially isoenergetic. Thus, there is a much smaller ΔE_{ST} value of 0.08 eV for **2B-DTACrs** compared to 0.20 eV of **1B-DTACrs**. The oscillator strength (f) for the S_0–S_1 transition is higher at 0.36 for **2B-DTACrs** compared to 0.23 for **1B-DTACrs** likely for the apparent largest delocalization of the S_1 excited state. Both the S_2 and T_2 states of **2B-DTACrs** are also stabilized compared to those of **1B-DTACrs**. The small energy difference between S_1 and T_2 (ΔE_{ST_2}) is of particular interest as many reports have highlighted that reverse intersystem crossing (RISC) occurs *via* intermediate triplet states.[16] The ΔE_{ST_2} drops from 0.34 eV in **1B-DTACrs** to 0.02 eV in
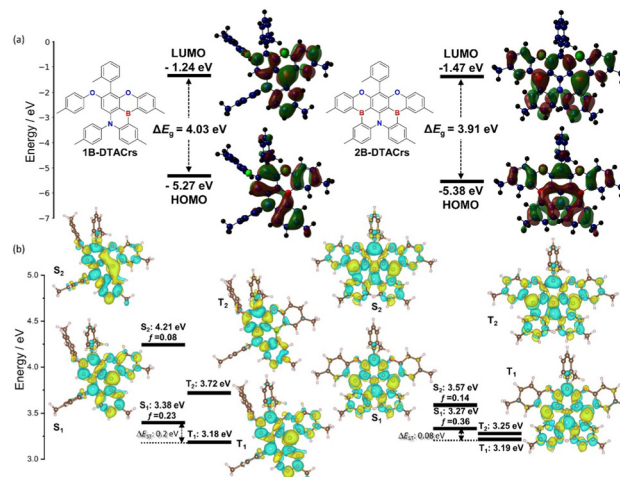

Fig. 2 (a) HOMO (bottom) and LUMO (top) electron density distributions of **1B-DTACrs** (left) and **2B-DTACrs** (right) calculated using PBE0/6-31G(d,p) (isovalue = 0.02). (b) Difference density plots for the low-lying singlet and triplet excited states for **1B-DTACrs** and **2B-DTACrs** calculated in the gas phase using SCS-CC2/pVDZ (isovalue = 0.001). Blue colour represents an area of decreased electron density, and yellow represents an increased electron density between the ground and excited states. f denotes the oscillator strength for the transition to the excited singlet state.

2B-DTACrs. For each compound, spin-orbital coupling (SOC) is modest between S_1 and T_1, calculated to be 0.07 cm^{-1} and 0.04 cm^{-1} for **1B-DTACrs** and **2B-DTACrs**, respectively. This increases to 0.81 cm^{-1} and 0.98 cm^{-1} between S_1 and T_2 for **1B-DTACrs** and **2B-DTACrs**, respectively (Table S3, ESI†). These results suggest that RISC likely proceeds from T_2 to S_1, particularly for **2B-DTACr**.[17] Tables S1–S3 (ESI†) provide a full summary of the excited state energies, transitions and SOC values.

The electrochemical properties were measured using cyclic voltammetry (CV) and differential pulse voltammetry (DPV) in deaerated dichloromethane (DCM) with 0.1 M tetra-*n*-butylammonium hexafluorophosphate as the supporting electrolyte (Fig. S21 and Table S4, ESI†). The oxidation potentials, E^{ox}, determined from the peak of the first oxidation wave of the DPV, are 1.07 V and 1.17 V *versus* a saturated calomel electrode (SCE), respectively, for **1B-DTACrs** and **2B-DTACrs**. The corresponding reduction potentials, E^{red}, are −2.10 V and −1.89 V, respectively, *versus* SCE for **1B-DTACrs** and **2B-DTACrs**. The corresponding HOMO and LUMO levels were calculated to be −5.42 eV and −2.24 eV for **1B-DTACrs**.[18] The HOMO and LUMO energy levels are stabilized to −5.51 eV and −2.46 eV, respectively, for **2B-DTACrs**. The electrochemical gap is thus reduced from 3.17 eV for **1B-DTACrs** to 3.05 eV for **2B-DTACrs**, in line with the trend predicted by the gas-phase DFT calculations.

The photophysical properties of **1B-DTACrs** and **2B-DTACrs** were firstly examined in dilute toluene solutions (10^{-5} M). The photophysical data are shown in Fig. 3, and Table 1. Both emitters showed absorption bands below 350 nm, which are assigned as locally excited (LE) π–π* transitions, while the absorption bands beyond 400 nm are assigned as short-range
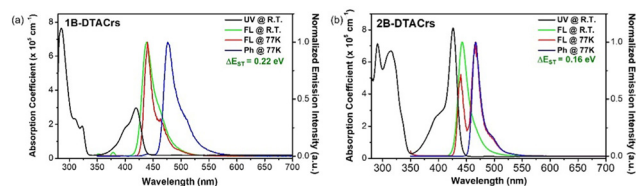
Fig. 3 Photophysical properties of (a) **1B-DTACrs** and (b) **2B-DTACrs** in toluene solution (10^{-5} M) at room temperature and 77 K (λ_{exc} = 280 nm and 320 nm for time-resolved and steady-state emission, respectively).

charge transfer (SRCT) bands. Both compounds possess narrow high-energy bands assigned to transitions to the S_1 state, with molar absorptivity coefficients, ε, of 3 and $8 \times 10^5 \, M^{-1} \, cm^{-1}$ for **1B-DTACrs** and **2B-DTACrs**, respectively, in line with the larger computed f associated with the $S_0 \rightarrow S_1$ transitions (*vide supra*). The higher calculated f value and measured ε in **2B-DTACrs** originates from the extended conjugation in the compound.[19] **1B-DTACrs** and **2B-DTACrs** emit in the deep-blue in toluene at 438 and 443 nm, respectively. The PL spectra of **1B-DTACrs** and **2B-DTACrs** are narrow with full-width at half-maxima (FWHM) values of 27 and 21 nm, respectively. The narrowband emission coupled with the small Stokes-shifts reflect the rigid nature of these compounds and the small degree of reorganization in the excited state. The Φ_{PL} in degassed toluene solutions of **1B-DTACrs** is 99%, while **2B-DTACrs** showed a rather lower Φ_{PL} of 62%. When doped in a 3,3′-di(9H-carbazol-9-yl)-1,1′-biphenyl (mCBP) host at 5 wt% of **1B-DTACrs** or **2B-DTACrs**, the Φ_{PL} values remain high at 83 and 74%, respectively. Both doped films display emissions (Fig. 4) solely originated from the corresponding emitter, which indicate an efficient energy transfer from mCBP to the emitter. The transient decay profiles of both doped films reveal that **1B-DTACrs** showed no TADF behaviour. By contrast, **2B-DTACrs** showed TADF behaviour with a delayed lifetime (τ_d) of 13.1 μs. The TADF behaviour of **2B-DTACrs** was further confirmed by temperature-dependent transient emission decay measurement (Fig. S22, ESI†). The ΔE_{ST} values of the mCBP doped films were determined from the difference between the onsets of the fluorescence and phosphorescence spectra at 77 K (Fig. S23, ESI†). The fairly large ΔE_{ST} in **1B-DTACrs**-doped film (0.21 eV) may account for the non-TADF behaviour while that of **2B-DTACrs** is smaller at 0.16 eV. The rate constants of doped films of **1B-DTACrs** and **2B-DTACrs** were calculated, and the data are summarized in Table 1. The reverse intersystem crossing rate (k_{RISC}) of **2B-DTACrs** was found to be $1.3 \times 10^5 \, s^{-1}$, which is amongst
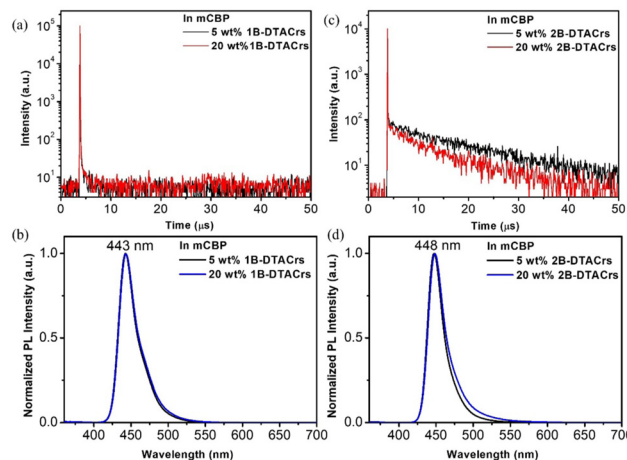

Fig. 4 Decay profiles and emission spectra of (a) and (b) **1B-DTACrs** and (c) and (d) **2B-DTACrs** at different doping concentrations in mCBP (λ_{exc} = 280 nm and 320 nm for time-resolved and steady-state emission, respectively).

the fastest k_{RISC} for deep-blue MR-TADF emitters with $CIE_y \leq 0.10$ (Table S5, ESI†).

We next fabricated vacuum-deposited OLEDs using **1B-DTACrs** and **2B-DTACrs** as the emitters. The following device configuration was used: indium-tin-oxide (ITO)-coated glass (100 nm)/HAT-CN (10 nm)/TAPC (30 nm)/mCP (10 nm)/mCP: 5 wt% of **1B-DTACrs** or **2B-DTACrs** (20 nm)/DPEPO (10 nm)/ TmPyPB (30 nm)/Liq (2 nm)/Al (100 nm). 1,4,5,8,9,11-Hexaazatriphenyl-enehexacarbonitrile (HAT-CN) is the hole-injection layer, 1,1-bis[(di-4-tolylamino)phenyl]cyclohexane (TAPC) is the hole-transporting layer, 1,3-bis(N-carbazolyl)benzene (mCP) is used for electron-blocking and host layers, bis[2-(diphenylphosphino)phenyl]ether oxide (DPEPO) is the hole-blocking layer, 1,3,5-tris(3-pyridyl-3-phenyl)benzene (TmPyPB) is the electron-transporting layer, and 8-hydroxyquinolinolato-lithium (Liq) and Al are the electron injection and cathode layers, respectively. Fig. 5, Fig. S24–S27 (ESI†) and Table 2 depict all the device characteristics. Devices based on **1B-DTACrs** (Device **I**) and **2B-DTACrs** (Device **II**) produced deep-blue narrowband emission at 440 and 447 nm, respectively, which are consistent to their corresponding PL spectra. The EL spectra clearly confirm the complete exciton confinement in both devices. The FWHM of Device **I** is 30 nm, which is slightly wider than that of Device **II** (FWHM = 26 nm). The corresponding $CIE_{x,y}$ are (0.154, 0.049) and (0.150, 0.044), respectively. Although the color gamuts of both devices are very close to the BT.2020 standard for the blue pixel, *i.e.*, (0.131, 0.046), the

Table 1 Photophysical data of **1B-DTACrs** and **2B-DTACrs**

Material	In toluene						5 wt% in mCBP											
	λ_{abs} (nm)	λ_{max} (nm)	FWHM (nm)	$\Phi_{Air}{}^a$ (%)	$\Phi_{Ar}{}^b$ (%)	ΔE_{ST} (eV)	λ_{max} (nm)	FWHM (nm)	ΔE_{ST} (eV)	Φ_{Ar} (%)	$\Phi_p{}^c$ (%)	$\Phi_d{}^d$ (%)	τ_p (ns)	τ_d (μs)	k_r ($10^8 \, s^{-1}$)	k_{nr} ($10^7 \, s^{-1}$)	k_{ISC} ($10^8 \, s^{-1}$)	k_{RISC} ($10^5 \, s^{-1}$)
1B-DTACrs	420	438	27	68	99	0.22	443	28	0.21	83	—	—	10	—	0.8	1.7	0.2	—
2B-DTACrs	425	443	21	20	64	0.16	448	24	0.16	74	35	39	2	13.1	1.7	6.1	3.3	1.3

[a] PLQY in aerated toluene. [b] PLQY in argon-saturated toluene. [c] Prompt intensity. [d] Delayed intensity.
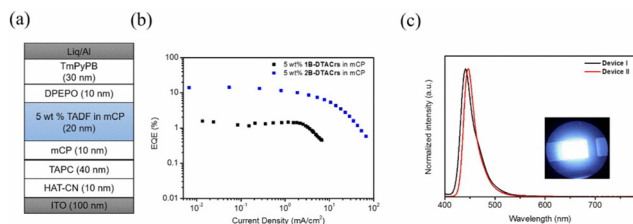
Fig. 5 Device performance of TADF OLEDs. (a) Device structure; (b) EQE *versus* current density; (c) EL spectra of devices at 10 cd m^{-2} (inset: photo of Device II).

Table 2 Device performance of deep-blue TADF OLEDs

Device	Dopant	$V_{on}{}^a$ (V)	$EQE_{max}{}^b$ (%)	$\lambda_{EL}{}^c$ (nm)	$FWHM^c$ (nm)	CIE^c (x, y)
I	**1B-DTACrs**	10	1.31	440	30	(0.154, 0.049)
II	**2B-DTACrs**	4	14.8	447	26	(0.150, 0.044)

^{a} Voltage at 1 cd m^{-2}. ^{b} Maximum external quantum efficiency. ^{c} Value at 10 cd m^{-2}.

efficiencies of two devices varied significantly. Taking advantage of enhanced exciton harvesting ability of **2B-DTACrs**, Device **II** demonstrated an excellent EQE$_{max}$ of 14.8%, which is one of the highest performing deep-blue MR-TADF OLEDs with CIE$_y$ ≤ 0.05 (Table S5, ESI†);[14] there is, however, considerable efficiency roll-off beyond 100 cd m^{-2}. By contrast, Device **I** only showed a poor EQE$_{max}$ of 1.3%, which is in part due to the fact that only singlet excitons can be utilized. Additionally, the poor carrier transporting properties in device I, in which a high turn-on voltage was obtained, may contribute to the lower EQE than the theoretical value (5%).

In conclusion, we presented two deep-blue p,n-doped nanographene emitters (**1B-DTACrs** and **2B-DTACrs**), in which **2B-DTACrs** with two boron atoms is TADF-active while **1B-DTACrs** with only one boron atom is TADF inactive. It is noteworthy that the emitter **2B-DTACrs** does not show red-shifted emission. Devices based on **2B-DTACrs** achieved a high EQE$_{max}$ of 14.8% and CIE$_{x,y}$ of (0.150, 0.044), which are one of highest efficiency deep-blue MR-TADF devices reported to date. Importantly, the CIE coordinates effectively meet the colour gamut requirement for the BT.2020 standard for the blue pixel.

Conflicts of interest

There are no conflicts to declare.

Notes and references

1 H. Uoyama, K. Goushi, K. Shizu, H. Nomura and C. Adachi, *Nature*, 2012, **492**, 234–238.
2 M. Y. Wong and E. Zysman-Colman, *Adv. Mater.*, 2017, **29**, 1605444.
3 D. H. Ahn, S. W. Kim, H. Lee, I. J. Ko, D. Karthik, J. Y. Lee and J. H. Kwon, *Nat. Photonics*, 2019, **13**, 540–546.
4 H. Kaji, H. Suzuki, T. Fukushima, K. Shizu, K. Suzuki, S. Kubo, T. Komino, H. Oiwa, F. Suzuki, A. Wakamiya, Y. Murata and C. Adachi, *Nat. Commun.*, 2015, **6**, 8476.
5 T.-L. Wu, M.-J. Huang, C.-C. Lin, P.-Y. Huang, T.-Y. Chou, R.-W. Chen-Cheng, H.-W. Lin, R.-S. Liu and C.-H. Cheng, *Nat. Photonics*, 2018, **12**, 235–240.
6 Y.-L. Zhang, Q. Ran, Q. Wang, Y. Liu, C. Hänisch, S. Reineke, J. Fan and L.-S. Liao, *Adv. Mater.*, 2019, **31**, 1902368.
7 T. Hatakeyama, K. Shiren, K. Nakajima, S. Nomura, S. Nakatsuka, K. Kinoshita, J. Ni, Y. Ono and T. Ikuta, *Adv. Mater.*, 2016, **28**, 2777–2781.
8 J.-M. Teng, Y.-F. Wang and C.-F. Chen, *J. Mater. Chem. C*, 2020, **8**, 11340–11353.
9 H. Lee, D. Karthik, R. Lampande, J. H. Ryu and J. H. Kwon, *Front. Chem.*, 2020, **8**, 373.
10 S. Madayanad Suresh, D. Hall, D. Beljonne, Y. Olivier and E. Zysman-Colman, *Adv. Funct. Mater.*, 2020, **30**, 1908677.
11 N. Ikeda, S. Oda, R. Matsumoto, M. Yoshioka, D. Fukushima, K. Yoshiura, N. Yasuda and T. Hatakeyama, *Adv. Mater.*, 2020, **32**, 2004072.
12 M. Yang, I. S. Park and T. Yasuda, *J. Am. Chem. Soc.*, 2020, **142**, 19468–19472.
13 Y. Zhang, D. Zhang, T. Huang, A. J. Gillett, Y. Liu, D. Hu, L. Cui, Z. Bin, G. Li, J. Wei and L. Duan, *Angew. Chem., Int. Ed.*, 2021, **60**, 20498–20503.
14 I. S. Park, M. Yang, H. Shibata, N. Amanokura and T. Yasuda, *Adv. Mater.*, 2022, **34**, 2107951.
15 M. Nagata, H. Min, E. Watanabe, H. Fukumoto, Y. Mizuhata, N. Tokitoh, T. Agou and T. Yasuda, *Angew. Chem., Int. Ed.*, 2021, **60**, 20280–20285.
16 I. Lyskov and C. M. Marian, *J. Phys. Chem. C*, 2017, **121**, 21145–21153.
17 S. M. Pratik, V. Coropceanu and J.-L. Brédas, *ACS Mater. Lett.*, 2022, **4**, 440–447.
18 N. G. Connelly and W. E. Geiger, *Chem. Rev.*, 1996, **96**, 877–910.
19 A. Pershin, D. Hall, V. Lemaur, J.-C. Sancho-Garcia, L. Muccioli, E. Zysman-Colman, D. Beljonne and Y. Olivier, *Nat. Commun.*, 2019, **10**, 597.